Article

Synthesis of a Poly-L-lysine/Black Phosphorus Hybrid for Biosensors

Yun Zhao, Ye-Hua Zhang, Zhen Zhuge, Yi-Hong Tang, Jian-Wei Tao, and Yong Chen

Anal. Chem., **Just Accepted Manuscript** • DOI: 10.1021/acs.analchem.7b04395 • Publication Date (Web): 05 Feb 2018

Synthesis of a Poly-L-lysine/Black Phosphorus Hybrid for Biosensors

Yun Zhao*, Ye-Hua Zhang, Zhen Zhuge, Yi-Hong Tang, Jian-Wei Tao, Yong Chen*

School of Chemical and Environmental Engineering, Shanghai Institute of Technology, Shanghai 201418, China.

Corresponding authors. Email: zhaoyun@sit.edu.cn (Y. Zhao); yongchen@sit.edu.cn (Y. Chen)

Tel: +86-21-60873241

ABSTRACT: A simple, non-covalent modification strategy was proposed to synthesized poly-L-lysine-black phosphorus (pLL-BP) hybrid. BP nanoflakes were prepared with a water-phase exfoliation method. pLL can adhere to the surface of BP *via* hydrophobic interaction between butyl chains of pLL and BP surface, as well as the electrostatic interaction between the protonated amino groups on pLL and the negative charge on deprotonated P_xO_y groups remaining on BP. The as-synthesized pLL-BP hybrid turns out to be an ideal matrix for hemoglobin immobilization and direct electron transfer. Good conductivity and biocompatibility of BP maintain the native structure and the bioactivity of hemoglobin (Hb), facilitating the direct electron transfer between the electroactive center of Hb and electrode. The rate constant (k_{ET}) for direct electron transfer of Hb@pLL-BP is calculated to be 11.24 s^{-1}. The constructed Hb-pLL-BP based enzymatic electrochemical biosensor displays excellent catalytic activity toward the reduction of oxygen and hydrogen peroxide. The electrochemical response toward H_2O_2 exhibits a linear dependence on hydrogen peroxide concentration ranging between 10 μM and 700 μM. The results demonstrate that the pLL-BP hybrid can act as a biocompatible building block for the construction of novel biofuel cells, bioelectronics and biosensors.

Two dimensional nanomaterials such as graphene and transition metal dichalcogenides (TMDCs) have attracted scientists' continuous attention for their desirable physical and structural properties[1-3], also their wide application in analytical chemistry[4-7]. However, in the past three years, an elemental layered material black phosphorus has triggered a renaissance of interest owing to its unique structure as well as fascinating optical and electronic properties. Black phosphorus (BP) was first mechanically exfoliated in success from bulk black phosphorus in 2014[8]. Unlike graphene, black phosphorus forms a puckered honeycomb orthorhombic lattice with each P atom bonded covalently with three adjacent P atoms, leaving a layer-to-layer space of approximately 5 Å[9-11]. This unique structure endows black phosphorus with fascinating electronic properties, such as high mobility[8,12-15], a layer-dependent tunable direct band gap[16,17], anisotropic electrical and thermal conductivities[18-20] as well as excellent optical response[21,22]. The unique electronic and optoelectronic properties make phosphorene a promising candidate in a variety of applications, including optoelectronic devices[23,24], solar cells[25,26], nanoelectronic devices[8,27], thermoelectric devices[28-30] and to name a few. Very recently, the synthesis of black phosphorus based composite has become a new trend[31-33]. A newest review on black phosphorus summarized BP's origins, physical and chemical properties, as well as the highlighted applications[34]. However, compared to the expanding growth on the development of various kinds of black phosphorus-based electronics and optoelectronics devices, the application research of black phosphorus toward sensing and biosensing field is still in its cradle, though several pioneering work have been done about using black phosphorus-based field-effect transistors for humidity sensing[35-37], gas sensing[38-40], or pollutant ions sensing[41,42].

Black phosphorus is a biocompatible[43], low cytotoxicity[44], two-dimensional nanomaterial, and as a result, it is regarded as a desirable candidate for biochemical analysis. Herein, we focus our attention on the electrochemical biosensing performance of black phosphorus. The electrochemical nature of black phosphorus was first disclosed by Pumera in 2015, indicating that black phosphorus bears an intrinsic oxidation peak located at about ~0.6 V (vs. Ag/AgCl) at neutral pH[45]. Since then, some intriguing works have been published about fabricating black phosphorus-based electrochemical sensors, including a myoglobin sensor[46] and a rabbit IgG sensor[47]. Despite its fascinating properties, exploration of black phosphorus for electrochemical sensing still remains limited. In particular, there is still less effort made to investigate the direct electron transfer of protein in BP-based biosensor, this may be caused by its susceptibility towards water and air[17]. Such degradation of black phosphorus by water vapor and oxygen will be further aggravated upon the irradiation of visible light[48]. Considering the developing track of its peers such as two-dimensional graphene and layered transition metal dichalcogenides, perhaps the combination of black phosphorus with other bio-friendly materials is a desirable way to establish biosensing platform with improved sensitivity and stability.

In the present work, a polymer poly-L-lysine (pLL) / black phosphorus assembly was synthesized with a simple, non-covalent method at room temperature. pLL is a antimicrobial, cationic polymer commonly used for cell growth and biomolecules sensing[49,50], and as a result, it can function as a bridge between BP and biomolecules. The non-covalent electrostatic interaction between BP and pLL not only reserve BP's originally puckered honeycomb structure and thus good conductivity, but enhance BP's stability and dispersion in aqueous solution as well, offering promising possibility for further biosensing. As demonstration, a negatively charged protein

hemoglobin (Hb) was immobilized on this pLL-BP hybrid, the immobilized protein displays excellent direct electron transfer (DET) and retains its outstanding biocatalytic activity toward the reduction of oxygen and hydrogen peroxide. For the best of our knowledge, it is the first time to report Hb's direct electron transfer on black phosphorus-based matrix. The result shows that pLL-BP hybrid is a promising building block in constructing novel biosensing and diagnostic platform for clinical and bioanalytical use.

EXPERIMENTAL SECTION

Reagents. Black phosphorus (BP) was purchased from Smart Elements. Poly-L-lysine hydrobromide (pLL, Mw~30000-70000), Hemoglobin (Hb, Mw ~64500 from bovine blood) and Nafion perfluorinated resin solution (5 wt% in mixture of low aliphatic alcohols and water, contains 45% water) were purchased from Sigma (USA). Hydrogen peroxide (H_2O_2, 30%) was purchased from Shanghai Sinopharm Chemical Reagent Co. Ltd. (China) and the stock solution was prepared freshly before use. Phosphate buffer solutions (PBS) were prepared by mixing KH_2PO_4 and K_2HPO_4, pH was modulated with concentrated HCl solution or NaOH solution. Other reagents were of analytical reagent grade and used as received. Deionized water purified from a Millipore-Q system (Milli-Q, Academic) was used in all the experiments.

Instrumentation. Raman spectra were measured using a DXR system equipped with a 532 nm laser operating at 1 mW (Termo Fisher Scientific, USA). Raman samples were prepared by drop casting 10 μL BP suspension on SiO_2 substrate. X-ray photoelectron spectroscopy (XPS) was performed with an ESCALAB 250Xi system (Termo Fisher Scientific, USA). XPS samples were prepared by drop casting 10 μL BP suspension on tinfoil substrate and dried in a N_2-filling glovebox. AFM images were acquired in peak force QNM mode using Bruker icon with Silicon nitride cantilever tip. The scanning rate for images taken was 1 Hz using an average of 256 or 384 samples per line (Bruker, German). AFM samples were freshly prepared and dried on a mica plate in N_2-filling glovebox. Transmission electron microscopy (TEM) images were obtained using a JEM-2100F system (JEOL, Japan). The samples were prepared by drying a droplet of sample suspensions on a Cu grid with carbon film. All the as-prepared samples for characterization were immediately transferred to the microscope or spectroscope after preparation, to minimize the photo-oxidative degradation. All the electrochemical analysis were carried out on a CHI 660E electrochemical workstation (CH Instrument Inc., USA) at ambient temperature with saturated calomel electrode (SCE) as the reference electrode, a platinum wire as the counter electrode and the modified glassy carbon electrode (GCE) as the working electrode. 20 mM pH 7.5 PBS was chosen as the electrolyte in all experiments.

Preparation of BP nanoflake. Bulk black phosphorus crystal was used as received. BP nanoflake was synthesized by a water-phase liquid exfoliation from corresponding bulk sample. In a typical procedure, 10 mg of the BP crystal was crushed into powder by mortar and pestle. Then the BP powder was dispersed in 10 mL deoxygenated distilled water and sealed with parafilm to avoid oxidation. The mixture solution was then sonicated in an ice-bath for 36 h. Afterward, the resultant brown suspension was centrifuged at 1500 rpm for 15 min to remove the residual unexfoliated particles and the supernatant was collected and further centrifuged at 3000 rpm, 5000 rpm sequentially. The supernatant of each centrifugation was collected for further use (noted as 3000-BP and 5000-BP, respectively).

Preparation of pLL-BP hybrid. To synthesis pLL-BP hybrid, 1 mL as-exfoliated BP dispersion was mixed with 2 mL 2 mg/mL pLL (prepared with deoxygenated distilled water) and the resultant mixture solution was then incubated for 12 h at 4 ℃.

Preparation of Hb-pLL-BP-GC electrode. A glassy carbon electrode (GCE) with a diameter of 3 mm was first mechanically polished with 0.3 μm and 0.5 μm alumina slurry sequentially and then sonicated in ethanol and deionized water for about 2 min. 5 μL as-synthesized pLL-BP hybrid was dropped onto the pretreated GCE and was dried in a N_2-filling glovebox. This pLL-BP-GC electrode (pLL-BP-GCE) was then used as an excellent matrix for protein immobilization.

For BP-based enzymatic biosensor fabrication, pLL-BP-GCE was first immersed in a 3 mg/mL Hb solution (prepared with 20 mM pH 8.0 PBS prior to use) for 12 h, dried in a N_2-filling glovebox, stepped by casting 1.0 μL Nafion solution on the electrode as a protective layer. The prepared Hb-pLL-BP-GCE was dried in a N_2-filling glovebox and kept at 4 ℃ when not use.

Electrochemical Measurements. The modified electrodes were characterized by electrochemical impedance spectroscopy (EIS). EIS was performed within the frequency range between 10^{-2} to 10^5 Hz, in 0.1 M KCl solution containing 10.0 mM $Fe(CN)_6^{3-}/Fe(CN)_6^{4-}$ (1:1) as the electrochemical probe. Direct electrochemistry and electrocatalytic performance of Hb were studied using cyclic voltammetry (CV) with conventional three-electrode configuration with a sweeping potential window ranging from +0.2 to -0.8 V at a scan rate of 500 mV/s. Amperometric i-t curve was used to evaluate the selectivity performance of the as-developed biosensor. In all electrochemical measurements, the buffer solution is 20 mM N_2-saturated PBS (pH 7.5) except for specific clarification.

RESULTS AND DISCUSSION

Characterization of BP nanoflakes. The morphology of exfoliated BP was studied with a transmission electron microscopy (TEM). Figure 1a and 1b display the TEM images of the exfoliated BP nanoflakes, showing free-standing few-layered nanoflakes with diameter of about one to several hundred nanometers. The size for 3000-BP is a little bit larger than that for 5000-BP, which may result from the fact that a faster centrifugation speed will accelerate the sedimentation of larger flakes. TEM result indicates that the exfoliated BP contains single to several ultrathin layers which is coincide to AFM results.

The thickness of the BP nanoflakes in the supernatant are further determined with atomic force microscopy (AFM). Figure S-1a to S-1d show the typical AFM images and height profiles for 3000-BP and 5000-BP, exhibiting an average height of about 4.0 nm for 3000-BP nanoflakes and 0.5 to 1.0 nm for 5000-BP nanoflakes. AFM results suggest that the exfoliated BP nanoflakes consist of about eight individual phosphorene layers for 3000-BP nanoflakes and one to two individual phosphorene layers for 5000-BP nanoflakes. In addition, the size of 5000-BP is a little bit smaller compared to that of 3000-BP, which may be again due to the sedimentation of larger nanoflakes caused by a relatively high centrifugation speed.

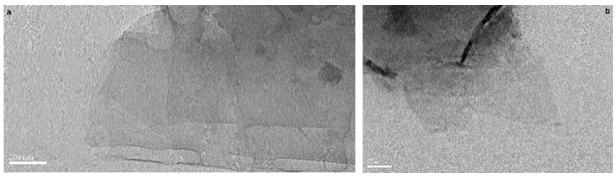

Figure 1. TEM image for the exfoliated BP nanoflakes centrifuged at a) 3000 rpm (3000-BP) and b) 5000 rpm (5000-BP).

Raman spectroscopy is an effective technique for sample identification by providing detailed vibrational and rotational modes. Figure 2 shows the structural transformation during water-phase liquid exfoliation process. Bulk BP exhibits three peaks located at about 361.8 cm^{-1}, 435.1 cm^{-1}, 463.1 cm^{-1}, corresponding to the out-of-plane vibrational mode A_g^1, in-plane vibrational mode B_{2g} and in-plane vibrational mode A_g^2. After exfoliation and centrifugation, these three distinct peaks shift to 364.7 cm^{-1}, 440.0 cm^{-1}, 466.9 cm^{-1} for the sample centrifuged at 3000 rpm and 365.7 cm^{-1}, 441.9 cm^{-1}, 470.8 cm^{-1} for that centrifuged at 5000 rpm, indicating the fact that exfoliated nanoflakes maintain the structure of corresponding bulk counterpart well. Moreover, the peak location is relevant to the layer thickness. Raman results show that three distinct peaks of BP exhibit a slight shift toward higher wavenumber with the decreasing of layer thickness, which is in accordance with the previous report[51,52]. We also discovered that among the three vibrational modes, A_g^2 mode turns out to be most sensitive to the layer number. After exfoliation, the A_g^2 mode shifts from 463.1 cm^{-1} to 470.8 cm^{-1} for 5000-BP nanoflakes while the A_g^1 mode and B_{2g} mode only have a 3.9 cm^{-1} and 6.8 cm^{-1} shift, respectively.

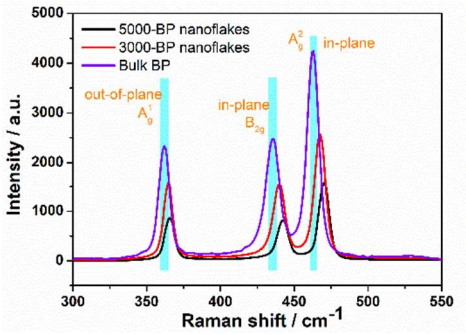

Figure 2. Raman spectra of bulk BP and exfoliated BP nanoflakes centrifuged at 3000 rpm and 5000 rpm.

X-ray photoelectron spectroscopy (XPS) was used to further evaluate the structural integrity and purity of exfoliated BP nanoflakes. Figure 3a and 3b are the survey spectrum and the P2p core-level spectrum of the exfoliated 3000-BP nanoflakes, respectively. Peaks located at 129.2 eV and 130.0 eV are attributed to the expected contributions from $P_{2p3/2}$ and $P_{2p1/2}$ components, the small peak presented at 133.0 eV is the contributions from P_xO_y species, presumably as a result of minor oxidation on the surface of the nanoflakes. These results reveal the presence and homogeneous distribution of P element in the sample, indicating the high purity of the nanoflakes. The two small peaks at around 490 eV is due to the Sn substrate used during XPS measurement, while another small peak presented at 532.1 eV is the contributions from O1s. Calculation shows that about ca. 2% of the phosphorus was oxidized, as estimated by peak integration software. The XPS spectra for 5000-BP nanoflake were similar to that for 3000-BP nanoflakes (data are not shown).

Collectively, all the above characterization results demonstrate that our water-phase exfoliation successfully yields high-quality, nearly unoxidized two-dimensional BP nanomaterials. And since BP centrifuged at 3000 rpm has a much larger size which may benefit its electrochemical performance, so 3000-BP was chosen as the electrode modification material in the following electrochemical study.

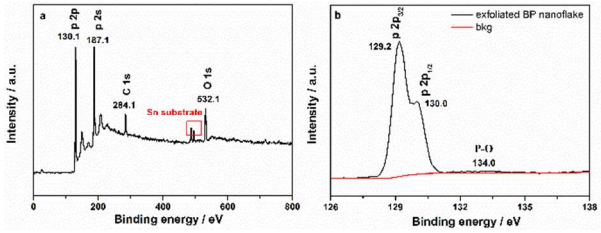

Figure 3. XPS spectra of exfoliated BP nanoflakes. a) Survey spectrum. b) XPS P2p core-level region.

Characterization of pLL-BP hybrid. Pristine BP is negatively charged with a zeta potential of about -23.4 mV[46] due to the partial deprotonation of the oxidized P_xO_y component. pLL is a cationic polymer with pK_a (-COOH) equals to 2.15, pK_a (-NH_3^+) equals to 10.67, and pK_a (ε -NH_2) equals to 9.16[53], so the isoelectric point PI of pLL is about 9.5[54]. Thus, due to the protonation of amine groups on polymer side chains, pLL should be positively charged in nearly neutral conditions. The resultant electrostatic interaction between pLL and BP contributes to their strong assembly. In addition, when adsorbing on 2D nanomaterials, it is more beneficial for pLL to expose its nonpolar parts (butyl chains with relatively hydrophobic properties) for interaction[55]. Therefore, besides the electrostatic interaction force, the hydrophobic force between the butyl chains and the surface of BP also contributes to the strong formation of pLL-BP hybrid. XPS was used to monitor the biofunctionalization strategy we adopted. In P2p core region (Figure S-2a), peak located at around 129 ~ 130 eV is attributed to the contribution of $P2p_{3/2}$ and $P2p_{1/2}$ components while that located near 133 eV is caused by P_xO_y component. The addition of pLL gives rise to a slight shift in binding energy toward higher values, with a small increase in the intensity of P_xO_y peak which may arise from some slight oxidation during the modification process. However, upon interaction with Hb, the BP-derived P2p signal is almost suppressed and is dominated by P_xO_y. The result is in accordance with the previous literature since the protein overlayer becomes comparable to the sampling depth of XPS[46], and also, the PBS buffer used in preparation of Hb solution contributed to the dramatic increase in P_xO_y constitution peak. In N1s core region (Figure S-2b), a broad N1s peak is observed in the pristine BP sample subjected to XPS analysis. The origin of the N1s signal is unknown, but the same phenomena was also reported in the previous work[46]. However, as is expected, XPS spectrum of pLL-BP hybrid exhibits a second, new peak at ~ 400 eV upon interaction with pLL, which is assigned to the amine in the lysine. The subsequent interaction with Hb brings a slight increase in the peak intensity and a subtle shift toward lower binding energy. In C1s core region (Figure S-2c), a small peak appears at ~ 288 eV after interaction with pLL and Hb, which arise from C−OH species. The slight increase in intensity indicates that

more C−OH will be present from pLL. The further binding with Hb brings about two new peak located at higher binding energy. The above overall XPS data summarize the substep assembly of Hb-pLL-BP biosensor.

Raman spectroscopy is quite sensitive to surface charge, layer numbers and structural defects[56]. In the present work, upon the non-covalent bonding of pLL, pLL-BP shows nearly identical peaks located at 364.6 cm^{-1}, 441.8 cm^{-1} and 469.7 cm^{-1}, which are assigned to the A_g^1, B_{2g} and A_g^2 phonons respectively. The stepped Hb immobilization brings about a slight red shift of approximately 1 cm^{-1} for all three peaks (Figure S-3). The above results indicates that non-covalent binding with pLL and Hb molecules dose not destroy BP's native structure, the oscillation of the P atoms of BP is restricted to some extent due to protein's large molecular weight, thus decreasing the corresponding Raman scattering energy[57-59].

Electrochemical impedance spectroscopy (EIS) is a useful technique to determine the interfacial properties between the electrode-electrolyte boundaries. The semicircular part at higher frequencies corresponds to the electron transfer limited process while the linear part at lower frequencies corresponds to the diffusion limited process. The diameter of the semicircle corresponds to the interfacial electron transfer resistance (R_{ct}), which reflects the electron-transfer kinetics of the redox probe at the electrode interface. In the present work, EIS was also used to probe electrode modification steps. Figure S-4 shows the Nyquist diagrams of bare GCE, BP-GCE, pLL-BP-GCE and Hb-pLL-BP-GCE in 0.1 M KCl solution containing 10 mM $Fe(CN)_6^{3-}/Fe(CN)_6^{4-}$ (1:1) as electrochemical probe. The results show that the bare glassy carbon electrode gives an electron-transfer resistance of about 180 Ω (Figure S-4, black curve), implying a very low electron-transfer resistance to the redox probe dissolved in the electrolyte. When modified with BP nanoflakes, the semicircle increases to 410 Ω compared to the bare GCE (Figure S-4, red curve), showing that the negative charge of the deprotonated P_xO_y groups on BP has a relative weak electrostatic repulsion to the redox probe. The further binding with pLL brings about an almost straight line (Figure S-4, blue curve), indicating Warburg resistance and the diffusion-limiting step in the electrochemical process[60] which may be attributed to the electrostatic attraction between positive-charged pLL and the negative-charged probe. However, when the pLL-BP modified electrode was incubated in Hb solution for certain time, the EIS shows a much higher interfacial electron-transfer resistance (Figure S-4, pink curve), indicating that the absorbed Hb molecules inhibit the effective electron transfer between $Fe(CN)_6^{3-}/Fe(CN)_6^{4-}$ and the electrode, possibly due to the electrostatic repulsion between negatively charged Hb and the electrochemical probe. These results confirm the successful assembly of pLL-BP hybrid and the immobilization of Hb on pLL-BP film.

Direct electrochemistry of Hb@pLL-BP hybrid modified GC electrode. The isoelectric point (pI) of Hb equals to 6.93[61]. Since pLL-BP hybrid has a positively charged surface in 20 mM PBS solution (pH 7.5), as a result, the negatively charged Hb can be embedded into the hybrid *via* electrostatic interaction. In addition, the hydrogen bonding between partially BP oxidized configuration P_xO_y on BP surface and -NH_2 group on Hb protein also contributes to the protein immobilization. Hb is a heme protein containing four electroactive iron hemes, which is often used as an ideal model to study the electron transfer of heme proteins due to its key role in oxygen transport. Figure 4a are the cyclic voltammograms for the modified electrodes of each modification step. As is expected, pLL-BP-GCE exhibits no Faradic features except for the double layer charging (Figure 4a, black curve). When embedded with Hb, Hb-pLL-BP-GCE shows a pair of well-defined and quasi-reversible redox peaks (Figure 4a, red curve). The observed formal potential $E^{0\prime}$ [$E^{0\prime}$= (E_{pa}+E_{pc})/2] is calculated to be -0.387 V (*vs*. SCE), which is in accordance with that for the heme redox couple within Hb reported previously[62-65]. The results present strong evidence to show that direct electron transfer between immobilized Hb and GCE can be achieved by using pLL-BP hybrid as a matrix. The peak to peak separation value ($\triangle E_p$) is about 69 mV, indicating a fast electron transfer process. It is worthy to note that without BP, Hb exhibits a rather poor electron transfer behavior on pLL-GCE (Figure 4a, blue curve), the symmetry of the redox peak become worse while the peak current of Hb is almost one-third that of Hb on pLL-BP-GCE, indicating that the doping of BP facilitates the loading of protein molecules. Peak potential, $\triangle E_p$ and the formal potential $E^{0\prime}$ for each case are summarized in Table S-1. The peak current ratio (i_{pc}/i_{pa}) is calculated to be 1.02 for Hb@pLL-BP modified electrode while only reaches 1.60 for Hb@pLL modified electrode. The peak to peak separation value ($\triangle E_p$) increases from 69 mV for Hb@pLL-BP to 102 mV for Hb@pLL. These results demonstrate that Hb exhibits a much quicker and more reversible direct electron transfer @pLL-BP. Hb's efficient direct electron transfer on electrode doping with BP, may be attributed to BP's metallic character in the edges as the edges bear a significant higher electrochemical activity than the basal plane[66]. Cyclic voltammograms of Hb-pLL-BP-GCE in the same solution at different scan rate were then collected. Figure 4b and 4c show that the anodic and cathodic current exhibit a linear dependence on the scan rate ranging from 0.1 V/s to 10 V/s, indicating that the direct electron transfer of immobilized Hb in pLL-BP matrix corresponds to a surface-controlled process. According to the Laviron's equation[67], the rate constant (k_{ET}) of direct electron transfer can be determined from peak-to-peak separations shown in Figure 4d, assuming the charge-transfer coefficient α = 0.5 and the number of electrons (n =1) for one electron transfer process, k_{ET} is calculated to be 11.24 s^{-1}, which is twice the value of k_{ET} for Hb's DET on pLL-graphene modified electrode[55]. To the best of our knowledge, it is the first time to report direct electron transfer of Hb on BP-based hybrid. The observed direct electrochemistry of Hb@pLL-BP hybrid indicates that pLL-BP nanocomposite can offer a favorable microenvironment for the protein direct electron transfer. The inner space within the puckered honeycomb layers functions as a protect shell which prevent the immobilized protein from denaturing. Simultaneously, the doping of BP makes more active sites of Hb expose to the electrode, cutting the electron tunneling path for the direct electron transfer, and allow DET occur. Moreover, the phosphoric group of BP is also expected to contribute to quick DET of the immobilized proteins[65]. This intriguing direct electron transfer behavior inspires us to explore the biosensing performance of the as-synthesized Hb@pLL-BP.

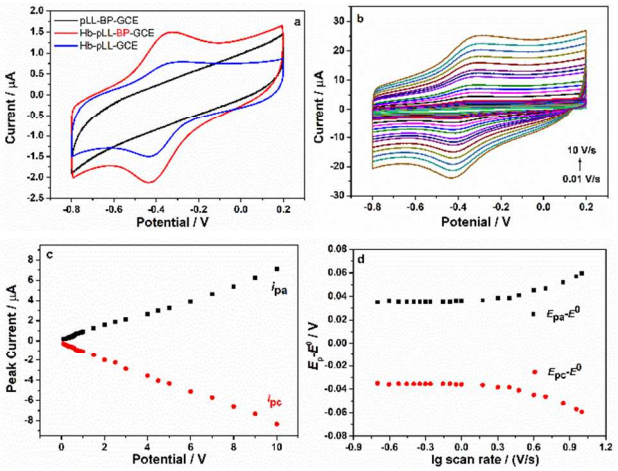

Figure 4. a) Cyclic voltammograms (CVs) of Hb-pLL-BP-GCE, pLL-BP-GCE and Hb-pLL-GCE in 20 mM pH 7.5 PBS at a scan rate of 500 mV•s^{-1}; b) Cyclic voltammograms (CVs) of Hb-pLL-BP-GCE in 20 mM pH 7.5 PBS at different scan rate ranging from 0.1 V•s^{-1} to 10 V•s^{-1}; c) Plot of i_p as a function of scan rate υ; d) Plot of (E_p-E^0) as a function of lgυ.

Electrocatalytic activity of Hb-pLL-BP toward oxygen reduction and hydrogen peroxide reduction. As a proof of concept in constructing BP-based enzymatic biosensors, we studied the electrochemical performance of Hb@pLL-BP toward oxygen reduction first. Figure 5a shows the cyclic voltammograms of Hb-pLL-BP-GCE in 20 mM PBS (pH 7.5) filling with N_2, air or O_2. In the solution saturated with N_2, since the dissolved concentration of O_2 can be negligible, a pair of well-defined and symmetric redox peaks can be recognized which is assigned to the direct electron transfer between Hb and the electrode (Figure 5a, black curve and inset). However, when the same measurement was carried out in air atmosphere, there is a small increase in the reduction current, and a simultaneous decrease in the oxidation current, which is due to the limited O_2 reduction catalyzed by Hb (Figure 5a, blue curve). Upon the addition of saturated O_2, there is a dramatic increase in the reduction peak current, accompanied by the disappearance of heme's oxidation peak, which is the typical catalytic behavior of Hb toward oxygen reduction (Figure 5a, red curve), indicating the fact that the redox of ferric/ferrous of the active center of Hb mediates the catalytic reduction of oxygen. In the control experiment (Figure 5b), without BP doping, although Hb can adsorb on pLL through electrostatic interaction, Hb tends to experience a native structural change which greatly deteriorates its catalytic activity. The electrocatalytic current of Hb-pLL-BP modified electrode toward oxygen reduction is almost 18 folds that of Hb-pLL modified electrode. The above results indicate that BP plays an indispensable role in the electrocatalytic performance of Hb which may be attributed to its good conductivity and unique two dimensional structure that offers a preferable microenvironment for protein to keep its native structure and inherent bioactivity.

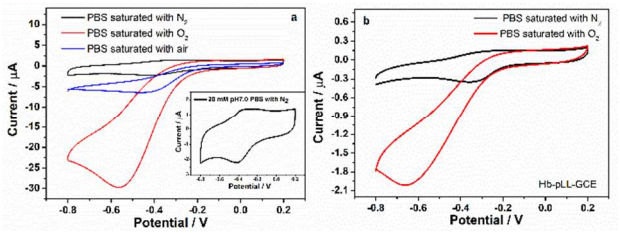

Figure 5. Cyclic voltammogram of a) Hb-pLL-BP-GCE, b) Hb-pLL-GCE in 20 mM pH 7.5 PBS saturated with N_2, air or O_2 at a scan rate of 0.5 V/s; inset in a) is the cyclic voltammogram of Hb-pLL-BP-GCE in N_2-saturated PBS.

According to the above results, BP provides a desirable microenvironment for the immobilization and direct electron transfer between Hb and electrode, so it is a very promising candidate for H_2O_2 biosensor. We then carefully studied the electrocatalytic activity of Hb-pLL-BP modified GC electrode toward the reduction of H_2O_2. As shown in Figure 6a, direct electron transfer of Hb can be seen in PBS solution saturated with N_2, however, upon the addition of 2 mM H_2O_2, the reduction current increases considerably, accompanied by the disappearance of oxidation peak. It is reasonable to think that the catalytic current comes from the interaction between Hb and H_2O_2. The catalytic reduction of hydrogen peroxide is mediated by the redox of ferric/ferrous of the active center of Hb. In contrast, the catalytic reduction current of pLL-BP toward the same amount of H_2O_2 is small enough to be neglected (Figure 6b, black dashed line). It is worthy to note that without the doping of BP, Hb-pLL modified GCE though exhibits some electrocatalytic activity toward H_2O_2 reduction, the starting cathodic reduction potential is more negative, and the catalytic current is rather smaller (Figure 6b, red dashed line), merely one-seventh compared to that of Hb-pLL-BP modified GCE (Figure 6b, blue dashed line), which again, confirms the indispensable role of BP in constructing enzymatic biosensors. The negative peak shift reflects the different microenvironment around protein molecules in different matrix. The larger catalytic current of Hb@pLL-BP indicates a more efficient DET between Hb and electrode and thus a more efficient catalytic activity. These results indicate that Hb can well retain its native structure @pLL-BP hybrid thanks to BP's honeycomb layered structure and exhibits a desirable electrocatalytic activity toward its substrate. The as-synthesized pLL-BP nanocomposite therefore can become an ideal matrix for protein loading and biocatalysis.

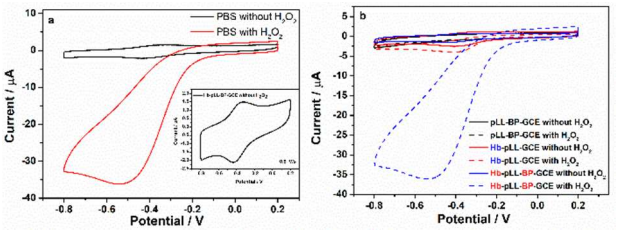

Figure 6. Cyclic voltammograms of a) Hb-pLL-BP modified electrode, b) pLL-BP, Hb-pLL and Hb-pLL-BP modified electrode in 20 mM pH 7.5 PBS saturated with N_2 before and after adding 2 mM H_2O_2, the scan rate is 0.5 V/s; inset in a) is cyclic voltammogram of Hb-pLL-BP modified electrode immersed in PBS without H_2O_2.

Figure 7 shows the cyclic voltammograms of Hb-pLL-BP modified GC electrode in pH 7.5 PBS containing different

concentration of H_2O_2. The cathodic peak current increases with the increasing H_2O_2 concentration. The electrochemical responses show good linear relationship with H_2O_2 concentration ranging from 10 μM to 700 μM (Figure 7, inset). And finally, the selectivity of the as-prepared biosensor was studied. Figure 8 is the Amperometric response of Hb-pLL-BP modified GC electrode toward H_2O_2, uric acid (UA) and ascorbic acid (AA) at a detection potential of -0.25 V. The addition of 100 μM H_2O_2 leads to a steep increase in reduction peak current and achieved 90% of steady-state current within 1.0 s. While the addition of 500 μM UA and 500 μM AA do not cause any increase in peak current, indicating that the as-prepared biosensor has a good selectivity toward H_2O_2.

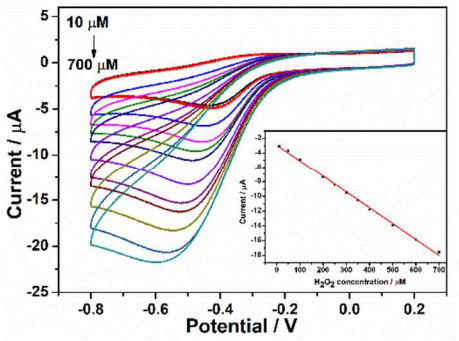

Figure 7. Cyclic voltammograms of Hb-pLL-BP modified electrode in 20 mM pH 7.5 PBS containing different H_2O_2 concentration at a scan rate of 0.5 V/s. The inset is the plot of cathodic peak current as a function of H_2O_2 concentration.

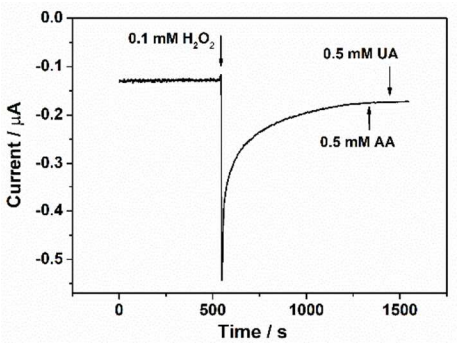

Figure 8. Amperometric response of Hb-pLL-BP electrode upon successive addition of 0.1 mM H_2O_2, 0.5 mM AA and 0.5 mM UA at -0.25 V under stirring in 20 mM pH 7.5 PBS saturated with N_2 at a scan rate of 0.5 V/s.

CONCLUTION

In summary, a new strategy to prepare a highly biocompatible pLL-BP hybrid is proposed. BP nanoflakes were prepared by a water-phase exfoliation in aqueous media. The assembly of pLL on BP surface is primarily driven by the synergetic effect of electrostatic interaction and hydrophobic interaction. The non-covalent functionalization of pLL improves BP's stability while maintain its good conductivity. The as-synthesized pLL-BP hybrid turns out to be a desirable matrix for protein direct electron transfer. Well-defined direct electrochemical behaviors of Hb-pLL-BP modified electrode suggest that the doping of BP makes the active sites of Hb exposure which allows DET occur. The as-demonstrated BP-based enzymatic biosensor shows good electrocatalytic activity toward oxygen reduction and hydrogen peroxide reduction. The results suggest that pLL-BP hybrid not only functions as a good electrical conductor, but also serves as a friendly biocompatible matrix which provides a favorable microenvironment for the immobilized protein to retain its biological activity and achieve fast direct electron transfer, and thus becoming a promising building blocks for novel biosensors and bioelectronics.

ASSOCIATED CONTENT

Supporting Information

Additional information as noted in text, including AFM images for exfoliated BP, XPS and Raman spectra of BP nanoflakes, pLL-BP and Hb-pLL-BP nanohybrid, EIS results for GCE, BP-GCE, pLL-BP-GCE and Hb-pLL-BP-GCE, and also the data of Hb's DET occurring on different modified electrodes. This Supporting Information is available free of charge on the ACS Publications website.

AUTHOR INFORMATION

Corresponding Author

*** Tel: +86-21-60873241; E-mail: zhaoyun@sit.edu.cn (Y. Zhao); yongchen@sit.edu.cn (Y. Chen)**

Notes

The authors declare no competing financial interest.

ACKNOWLEDGMENT

This research was supported by the National Natural Science Foundation of China (Grant no. 21605103), Open Foundation of State Key Laboratory of Analytical Chemistry for Life Science of Nanjing University (Grant no. SKLACLS1707).

REFERENCES

(1) Geim, A. K.; Novoselov, K. S. *Nat. Mater.* **2007**, *6*, 183-191.
(2) Novoselov, K. S.; Falko, V. I.; Colombo, L.; Gellert, P. R.; Schwab, M. G.; Kim, K. *Nature* **2012**, *490*, 192-200.
(3) Wang, Q. H.; Kalantar-Zadeh, K.; Kis, A.; Coleman, J. N.; Strano, M. S. *Nat. Nanotechnol.* **2012**, *7*, 699-712.
(4) Keun Soo, K.; Yue, Z.; Houk, J.; Yoon, L. S.; Jong Min, K.; Kim, K. S.; Jong-Hyun, A.; Philip, K.; Jae-Young, C.; Byung Hee, H. *Nature* **2009**, *457*, 706-710.
(5) Shao, Y.; Wang, J.; Wu, H.; Liu, J.; Aksay, I. A.; Lin, Y. *Electroanalysis* **2010**, *22*, 1027-1036.
(6) Kumar, B.; Min, K.; Bashirzadeh, M.; Farimani, A. B.; Bae, M. H.; Estrada, D.; Kim, Y. D.; Yasaei, P.; Park, Y. D.; Pop, E.; Aluru, N. R.; Salehi-Khojin, A. *Nano Lett.* **2013**, *13*, 1962-1968.
(7) Oriol, L. S.; Dominik, L.; Metin, K.; Aleksandra, R.; Andras, K. *Nat. Nanotechnol.* **2013**, *8*, 497-501.
(8) Li, L.; Yu, Y.; Ye, G. J.; Ge, Q.; Ou, X.; Wu, H.; Feng, D.; Chen, X. H.; Zhang, Y. *Nat. Nanotechnol.* **2014**, *9*, 372-377.
(9) Brown, A.; Rundqvist, S. *Acta Crystallogr.* **1965**, *19*, 684-685.
(10) Zhang, C. D.; Lian, J. C.; Yi, W.; Jiang, Y. H.; Liu, L. W.; Hu, H.; Xiao, W. D.; Du, S. X.; Sun, L. L.; Gao, H. J. *J.Phys.Chem.C* **2009**, *113*, 18823-18826.
(11) Cartz, L.; Srinivasa, S. R.; Riedner, R. J.; Jorgensen, J. D.; Worlton, T. G. *J. Chem. Phys.* **1979**, *71*, 1718-1721.
(12) Liu, H.; Neal, A. T.; Zhu, Z.; Luo, Z.; Xu, X.; Tománek, D.; Ye, P. D. *ACS Nano* **2014**, *8*, 4033-4041.
(13) Xia, F.; Wang, H.; Jia, Y. *Nat. Commun.* **2014**, *5*, 4458-4463.
(14) Koenig, S. P.; Doganov, R. A.; Schmidt, H.; Castro Neto, A. H.; Ozyilmaz, B. *Appl. Phys. Lett.* **2014**, *104*, 103104-103106.
(15) Churchill, H. O. H.; Jarillo-Herrero, P. *Nat. Nanotechnol.* **2014**, *9*, 330-331.
(16) Kim, J.; Baik, S. S.; Ryu, S. H.; Sohn, Y.; Park, S.; Park, B. G.; Denlinger, J.; Yi, Y.; Choi, H. J.; Kim, K. S. *Science* **2015**, *349*, 723-726.
(17) Castellanos-Gomez, A. *J Phys Chem Lett* **2015**, *6*, 4280-4291.

(18) Luo, Z.; Maassen, J.; Deng, Y. X.; Du, Y. C.; Garrelts, R. P.; Lundstrom, M. S.; Ye, P. D.; Xu, X. F. *Nat. Commun.* **2015**, *6*, 8572-8579.

(19) Lee, S.; Yang, F.; Suh, J.; Yang, S. J.; Lee, Y.; Li, G.; Choe, H. S.; Suslu, A.; Chen, Y. B.; Ko, C.; Park, J.; Liu, K.; Li, J. B.; Hippalgaonkar, K.; Urban, J. J.; Tongay, S.; Wu, J. Q. *Nat. Commun.* **2015**, *6*, 8573-8579.

(20) Ong, Z.-Y.; Cai, Y.; Zhang, G.; Zhang, Y.-W. *J. Phys. Chem. C* **2014**, *118*, 25272-25277.

(21) Fei, R.; Yang, L. *Nano Lett.* **2014**, *14*, 2884-2889.

(22) Tran, V.; Soklaski, R.; Liang, Y.; Yang, L. *Phys. Rev. B* **2014**, *89*, 235319-235325.

(23) Engel, M.; Steiner, M.; Avouris, P. *Nano Lett.* **2014**, *14*, 6414-6417.

(24) Youngblood, N.; Chen, C.; Koester, S. J.; Li, M. *Nat. Photonics* **2015**, *9*, 247-252.

(25) Dai, J.; Zeng, X. C. *J. Phys. Chem. Lett.* **2014**, *5*, 1289-1293.

(26) Buscema, M.; Groenendijk, D. J.; Steele, G. A.; Hs, V. D. Z.; Castellanos-Gomez, A. *Nat. Commun.* **2014**, *5*, 4651-4656.

(27) Miao, J.; Zhang, S.; Cai, L.; Scherr, M.; Wang, C. *ACS Nano* **2015**, *9*, 9236-9243.

(28) Fei, R.; Faghaninia, A.; Soklaski, R.; Yan, J. A.; Lo, C.; Yang, L. *Nano Lett.* **2014**, *14*, 6393-6399.

(29) Buscema, M.; Groenendijk, D. J.; Blanter, S. I.; Steele, G. A.; van der Zant, H. S. J.; Castellanos-Gomez, A. *Nano Lett.* **2014**, *14*, 3347-3352.

(30) Lv, H. Y.; Lu, W. J.; Shao, D. F.; Sun, Y. P. *Phys. Rev. B* **2014**, *90*, 085433-085440.

(31) Li, D.; Del Rio Castillo, A. E.; Jussila, H.; Ye, G.; Ren, Z.; Bai, J.; Chen, X.; Lipsanen, H.; Sun, Z.; Bonaccorso, F. *Applied Mater. Today* **2016**, 4, 17-23.

(32) Maric, T.; Moo, J. G. S.; Khezri, B.; Sofer, Z.; Pumera, M. *Applied Mater. Today* **2017,** 9, 289-291.

(33) Sofer, Z.; Luxa, J.; Bouša, D.; Sedmidubský, D.; Lazar, P.; Hartman, T.; Hardtdegen, H.; Pumera, M. *Angew. Chem. Int. Ed.* **2017,** 56, 9891-9896.

(34) Gusmão, R.; Sofer, Z.; Pumera, M. *Angew. Chem. Int. Ed. Engl.* **2017,** 56, 8052-8072.

(35) Yasaei, P.; Behranginia, A.; Foroozan, T.; Asadi, M.; Kim, K.; Khalili-Araghi, F.; Salehi-Khojin, A. *ACS Nano* **2015**, *9*, 9898-9905.

(36) Mayorga-Martinez, C. C.; Sofer, Z.; Pumera, M. *Angew. Chem., Int. Ed.* **2015**, *54*, 14317-14320.

(37) Sofer, Z.; Bousa, D.; Luxa, J.; Mazanek, V.; Pumera, M. *Chem. Commun.* **2016**, *52*, 1563-1566.

(38) Hanlon, D.; Backes, C.; Doherty, E.; Cucinotta, C. S.; Berner, N. C.; Boland, C.; Lee, K.; Harvey, A.; Lynch, P.; Gholamvand, Z.; Zhang, S.; Wang, K.; Moynihan, G.; Pokle, A.; Ramasse, Q. M.; McEvoy, N.; Blau, W. J.; Wang, J.; Abellan, G.; Hauke, F. *Nat. Commun.* **2015**, *6*, 8563-8573.

(39) Cho, S.-Y.; Lee, Y.; Koh, H.-J.; Jung, H.; Kim, J.-S.; Yoo, H.-W.; Kim, J.; Jung, H.-T. *Adv. Mater.* **2016**, *28*, 7020-7028.

(40) Cui, S.; Pu, H.; Wells, S. A.; Wen, Z.; Mao, S.; Chang, J.; Hersam, M. C.; Chen, J. *Nat. Commun.* **2015**, *6*, 8632-8640.

(41) Li, P.; Zhang, D.; Jiang, C.; Zong, X.; Cao, Y. *Biosens. Bioelectron.* **2017**, *98*, 68-75.

(42) Li, P.; Zhang, D.; Liu, J.; Chang, H.; Sun, Y. E.; Yin, N. *ACS Appl. Mater.* **2015**, *7*, 24396-24402.

(43) Lee, H. U.; Park, S. Y.; Lee, S. C.; Choi, S.; Seo, S.; Kim, H.; Won, J.; Choi, K.; Kang, K. S.; Park, H. G. *Small* **2016**, *12*, 214-219.

(44) Latiff, N.; Zhe Teo, W.; Sofer, Z.; C. Fisher, A.; Pumera, M. *Chem. -Eur. J.* **2015**, *21,* 13991-13995.

(45) Wang, L.; Sofer, Z.; Pumera, M. *ChemElectroChem* **2015**, *2*, 324-327.

(46) Kumar, V.; Brent, J. R.; Shorie, M.; Kaur, H.; Chadha, G.; Thomas, A. G.; Lewis, E. A.; Rooney, A. P.; Nguyen, L.; Zhong, X. L.; Burke, M. G.; Haigh, S. J.; Walton, A.; McNaughter, P. D.; Tedstone, A. A.; Savjani, N.; Muryn, C. A.; O'Brien, P.; Ganguli, A. K.; Lewis, D. J., Sabherwal, P. *ACS Appl. Mater. Interface* **2016**, *8*, 22860-22868.

(47) Mayorga-Martinez, C. C.; Mohamad Latiff, N.; Eng, A. Y. S.; Sofer, Z.; Pumera, M. *Anal. Chem.* **2016**, *88*, 10074-10079.

(48) Favron, A.; Gaufrès, E.; Fossard, F.; Lévesque, P. L.; Phaneufl'Heureux, A.; Tang, N. Y.; Loiseau, A.; Leonelli, R.; Francoeur, S.; Martel, R. *Physics* **2014**, *1*, 708-712.

(49) Sundlass, N. K.; Raines, R. T. *Biochemistry* **2011**, *50*, 10293-10299.

(50) Edwards, C, R.; Dang, W.; Berger, S. L. *Biochemistry* **2011**, *50*, 10473-10483.

(51) Guo, Z.; Zhang, H.; Lu, S.; Wang, Z.; Tang, S.; Shao, J.; Sun, Z.; Xie, H.; Wang, H.; Yu, X.-F.; Chu, P. K. *Adv. Funct. Mater.* **2015**, *25*, 6996-7002.

(52) Ge, S. F.; Li, C. K.; Zhang, Z. M.; Zhang, C. L.; Zhang, Y. D.; Qiu, J.; Wang, Q. S.; Liu, J. K.; Jia, S.; Feng, J.; Sun, D. *Nano Lett.* **2015**, *15*, 4650-4656.

(53) Sauer, B. B.; Kampert, W. G.; McLean, R. S.; Monteiro, R. *J. Polym. Sci., Part B: Polym. Phys.* **2011**, *49*, 222-243.

(54) Morga, M.; Adamczyk, Z.; Godrich, S.; Ocwieja, M.; Papastavrou, G. *J. Colloid Interface Sci.* **2015**, *456*, 116-124.

(55) Wang, J.; Zhao, Y.; Ma, F.-X.; Wang, K.; Wang, F.-B.; Xia, X.-H. *J. Mater. Chem. B* **2013**, *1*, 1406-1413.

(56) Eckmann, A.; Felten, A.; Mishchenko, A.; Britnell, L.; Krupke, R.; Novoselov, K. S.; Casiraghi, C. *Nano Lett.* **2012**, *12*, 3925-3930.

(57) Zhao, Y. T.; Wang, H. Y.; Huang, H.; Xiao, Q. L.; Xu, Y. H.; Guo, Z. N.; Xie, H. H.; Shao, J. D.; Sun, Z. B.; Han, W. J.; Yu, X. F.; Li, P. H.; Chu, P. K. *Angew. Chem., Int. Ed.* **2016**, *55*, 5003-5007.

(58) Yang, B. C.; Wan, B. S.; Zhou, Q. H.; Wang, Y.; Hu, W. T.; Lv, W. M.; Chen, Q.; Zeng, Z. M.; Wen, F. S.; Xiang, J. Y.; Yuan, S. J.; Wang, J. L.; Zhang, B. S.; Wang, W. H.; Zhang, J. Y.; Xu, B.; Zhao, Z. S.; Tian, Y. J.; Liu, Z. Y. *Adv. Mater.* **2016**, *28*, 9408-9415.

(59) Sreeprasad, T. S.; Nguyen, P.; Kim, N.; Berry, V. *Nano Lett.* **2013**, *13*, 4434-4441.

(60) Ren, X.; Pickup, P. G. *J. Electroanal. Chem.* **1997**, *420*, 251-257.

(61) J. Beckwith, R. M. Bell, S. Beychock, *Biochemistry*, Vol. 1 (Ed: G. Zubay), Addison-Wesley, New York, **1984**, Ch. 2.

(62) Yue, R.; Lu, Q.; Zhou, Y. *Biosens. Bioelectron.* **2011**, *26*, 4436-4441.

(63) Zhu, Z.; Qu, L.; Niu, Q.; Zeng, Y.; Sun, W.; Huang, X. *Biosens Bioelectron*. **2011**, *26*, 2119-2124.

(64) Guo, H.-L.; Liu, D.-Y.; Yu, X.-D.; Xia, X.-H. *Sens. Actuators, B* **2009**, 139, 598-603.

(65) Chen, Y.; Yang, X.-J.; Guo, L.-R.; Li, J.; Xia, X.-H.; Zheng, L.-M. *Anal. Chim. Acta* **2009**, 644, 83-89.

(66) Sofer, Z.; Sedmidubský, D.; Huber, Š.; Luxa, J.; Bouša, D.; Boothroyd, C.; Pumera, M. *Angew. Chem., Int. Ed.* **2016**, *55*, 3382-3386.

(67) Laviron, E. J. *Electroanal. Chem.* **1979**, *101*, 19-28.

For TOC only

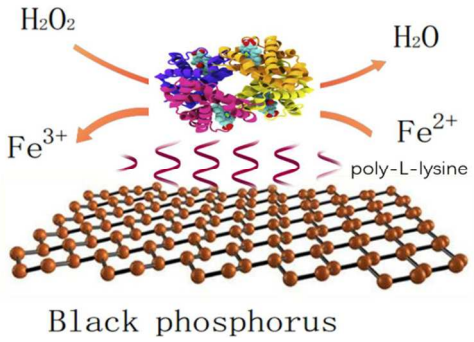
H_2O_2
H_2O
Fe^{3+}
Fe^{2+}
poly-L-lysine
Black phosphorus

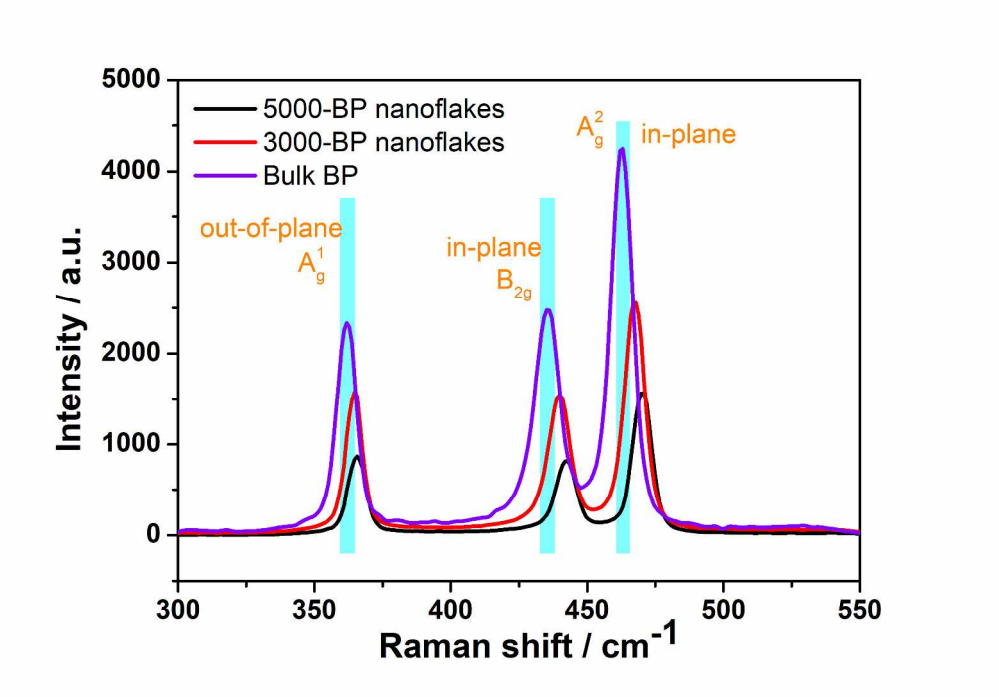

Figure 2. Raman spectra of bulk BP and exfoliated BP nanoflakes centrifuged at 3000 rpm and 5000 rpm.

289x201mm (300 x 300 DPI)

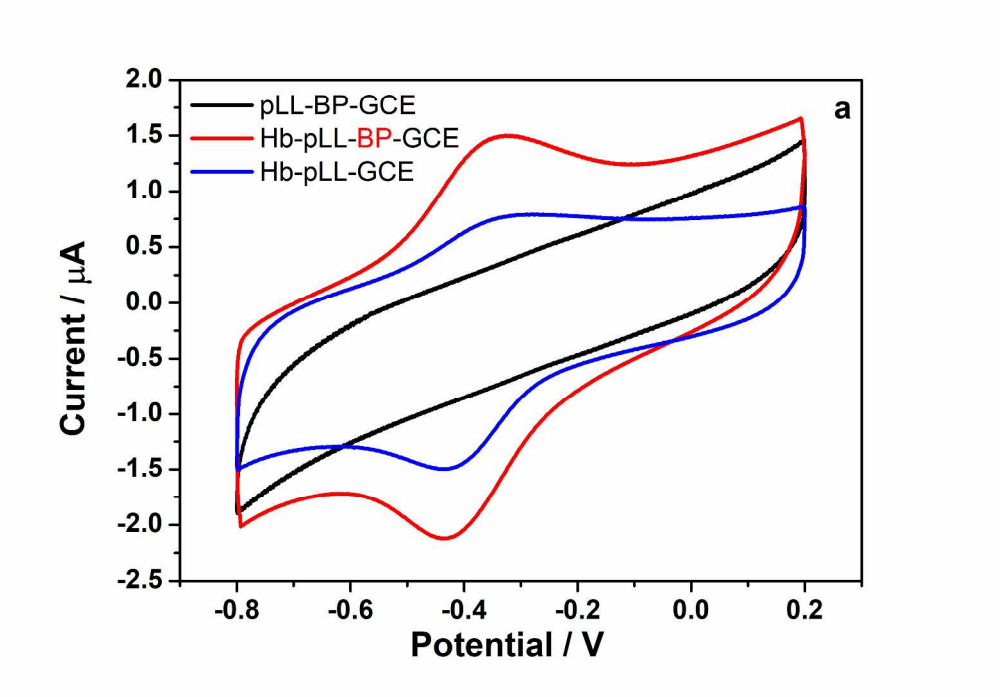

Figure 4. a) Cyclic voltammograms (CVs) of Hb-pLL-BP-GCE, pLL-BP-GCE and Hb-pLL-GCE in 20 mM pH 7.5 PBS at a scan rate of 500 $mV \bullet s^{-1}$;

289x201mm (300 x 300 DPI)

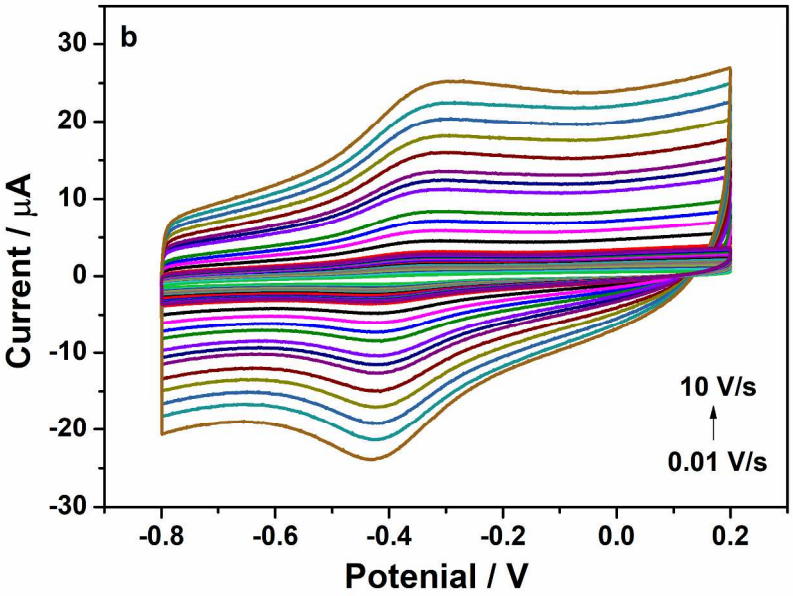

Figure 4. b) Cyclic voltammograms (CVs) of Hb-pLL-BP-GCE in 20 mM pH 7.5 PBS at different scan rate ranging from 0.1 V•s^{-1} to 10 V•s^{-1};

288x201mm (300 x 300 DPI)

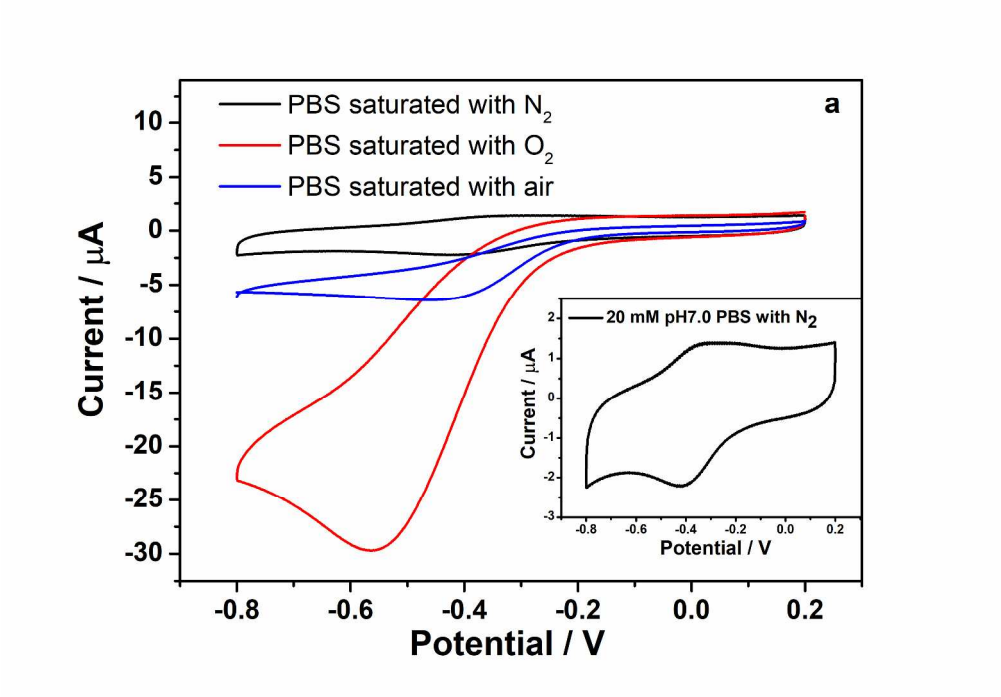

Figure 5a. Cyclic voltammogram of Hb-pLL-BP-GCE in 20 mM pH 7.5 PBS saturated with N_2, air or O_2 at a scan rate of 0.5 V/s; inset in a) is the cyclic voltammogram of Hb-pLL-BP-GCE in N_2-saturated PBS.

289x201mm (300 x 300 DPI)

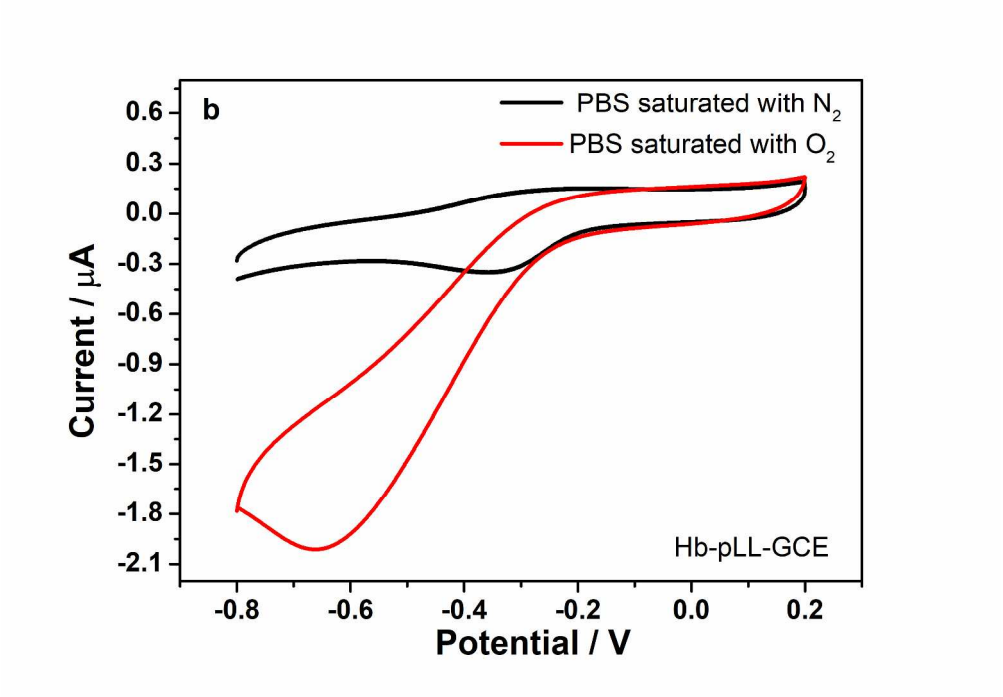

Figure 5b. Cyclic voltammogram of Hb-pLL-GCE in 20 mM pH 7.5 PBS saturated with N_2 or O_2 at a scan rate of 0.5 V/s;

289x201mm (300 x 300 DPI)

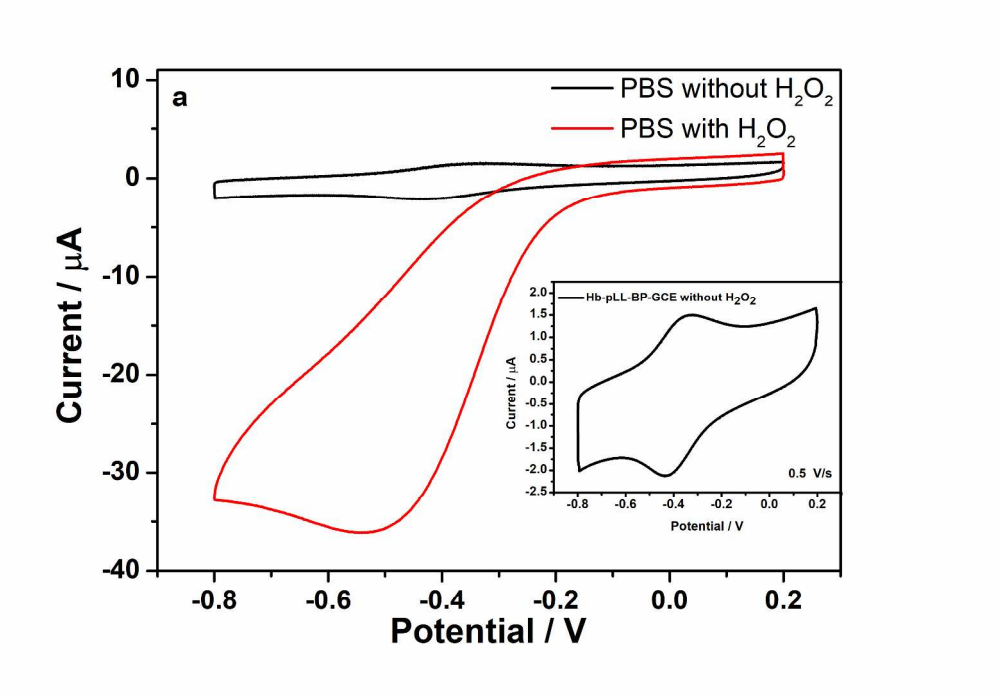

Figure 6a. Cyclic voltammograms of Hb-pLL-BP modified electrode in 20 mM pH 7.5 PBS saturated with N_2 before and after adding 2 mM H_2O_2, the scan rate is 0.5 V/s; inset in a) is cyclic voltammogram of Hb-pLL-BP modified electrode immersed in PBS without H_2O_2.

288x201mm (300 x 300 DPI)

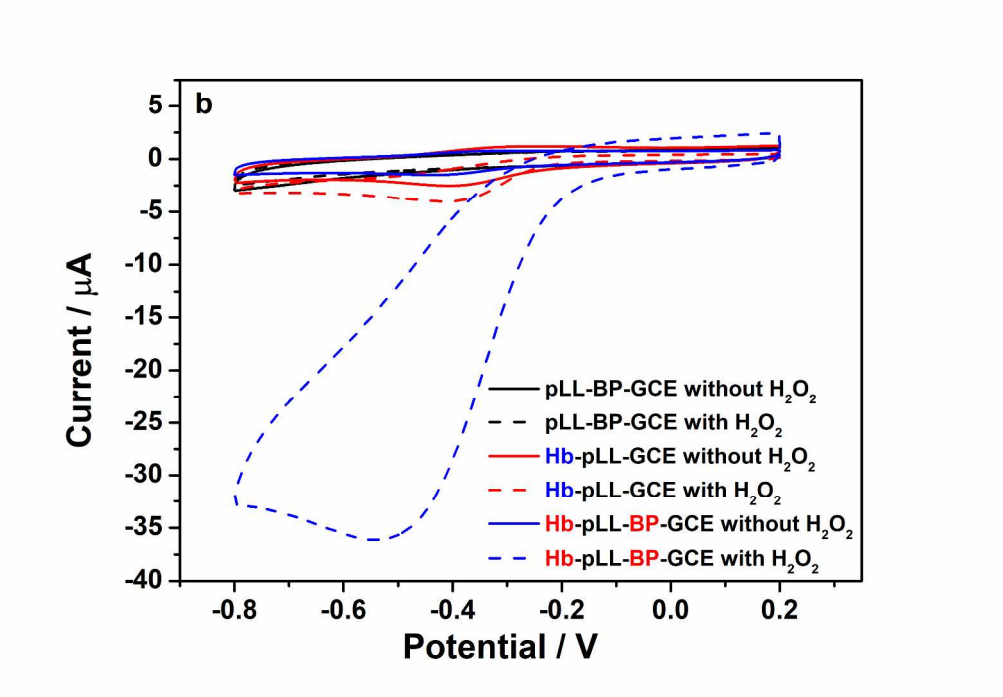

Figure 6b. Cyclic voltammograms of pLL-BP, Hb-pLL and Hb-pLL-BP modified elec-trode in 20 mM pH 7.5 PBS saturated with N_2 before and after adding 2 mM H_2O_2, the scan rate is 0.5 V/s;

289x201mm (300 x 300 DPI)